LASER PHYSICS LETTERS

www.lphys.org

EDITORIAL BOARD

W. Becker, Berlin
D. Chorvat, Bratislava
S. DeSilvestri, Milan
M. V. Fedorov, Moscow
A. Gaeta, Ithaca
S. A. Gonchukov, Moscow
M. Jelinek, Prague
U. Keller, Zürich
J. Lademann, Berlin
J. T. Manassah, New York
P. Meystre, Tucson
R. B. Miles, Princeton
P. P. Pashinin, Moscow
G. Petite, Saclay
L. P. Pitaevskii, Trento
M. Pollnau, Enschede
K. A. Prokhorov, Moscow
M. Scalora, Huntsville
V. M. Shalaev, West Lafayette
J. E. Sipe, Toronto
Ken-ichi Ueda, Tokyo
I. A. Walmsley, Oxford
E. Wintner, Vienna
E. Yablonovitch, Los Angeles
V. M. Yermachenko, Moscow
I. V. Yevseyev, Moscow
V. I. Yukalov, Dubna
A. M. Zheltikov, Moscow

REPRINT

Abstract: We have studied the surface-smoothing effect of an ultrathin germanium (Ge) layer on silver (Ag)-silica (SiO_2) nanocomposite films for superlensing applications. Our experimental results indicate that inserting a thin Ge layer below the silver-silica composite films can reduce the final surface root-mean-squared (RMS) roughness to under 1 nm. Additionally, the metal nanostructure plays a role in both the smoothing effect and the optical properties of the nanocomposite films. Our experimental results show that the Bruggeman effective medium theory (EMT) is not sufficiently accurate to describe some properties of our nanocomposite films. In addition to the constituent materials and their filling fraction within the composites, the detailed geometries of the metal nanostructures also show a significant influence on the optical properties of the composite films. This influence has not been taken into account by the EMT formulation.

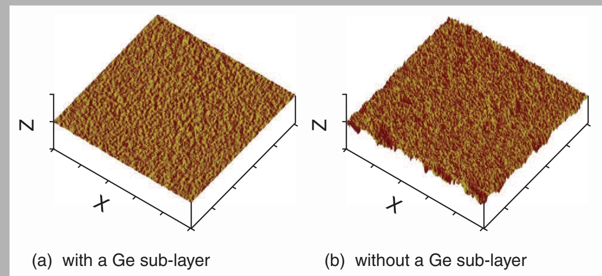

Surface morphologies from AFM topographs (a) 5 nm SiO_2/ 5 nm Ag composite film on a Ge/SiO_2/Si(100) substrate. (b) The same composite layers on a SiO_2/Si(100) substrate. The composite film (a) with a Ge sub-layer under it is smoother than the composite film (b) without a Ge sub-layer

© 2010 by Astro Ltd.
Published exclusively by WILEY-VCH Verlag GmbH & Co. KGaA

Fabrication and optical characterizations of smooth silver-silica nanocomposite films

W. Chen, [1,*] *M.D. Thoreson,* [2] *A.V. Kildishev,* [1] *and V.M. Shalaev* [1,*]

[1] Birck Nanotechnology Center and School of Electrical and Computer Engineering, Purdue University, West Lafayette, IN 47907, USA
[2] Erlangen Graduate School in Advanced Optical Technologies (SAOT), Universität Erlangen-Nürnberg, Erlangen 91052, Germany

Received: 29 April 2010, Revised: 30 April 2010 2010, Accepted: 3 May 2010
Published online: 30 June 2010

Key words: composite film; effective medium theory; superlens

1. Introduction

In the recent boom of metamaterials [1–9], the near-field superlens has attracted the interest of many theoretical and experimental researchers [10–16]. Near-field superlenses overcome Abbe's diffraction limit, a restriction on conventional lenses that limits the achievable resolution of imaged objects to about half of the incident light wavelength. This limitation occurs because conventional lenses with positive permittivity and permeability can only transmit the propagating-wave components of the source object. The evanescent waves that carry sub-wavelength information about the object will decay exponentially in such a positive-index medium and are lost before reaching the image plane, causing a limitation in the final image resolution. However, using a near-field superlens based on negative-index materials, the evanescent Fourier components from an object can grow exponentially and thus compensate for the exponential decay. Under ideal superlensing conditions, as suggested by J.B. Pendry [10], all Fourier components from the object can be recovered at the image plane and a resolution far below the diffraction limit can be achieved. Near-field superlensing occurs when the real part of the complex, frequency-dependent superlens permittivity $\varepsilon_{SL}(\omega)=\varepsilon'_{SL}(\omega)+i\varepsilon''_{SL}(\omega)$ satisfies the condition $\varepsilon'_{SL}(\omega)=-\varepsilon'_{H}(\omega)$, where $\varepsilon'_{H}(\omega)$ is the real part of the host material's complex permittivity [17, 18]. We note that developing the superlens is also important for a broader effort to advance artificial optical magnetism and the field of transformation optics [19–21].

* Corresponding author: e-mail: wqchen@purdue.edu; shalaev@purdue.edu

© 2010 by Astro Ltd.
Published exclusively by WILEY-VCH Verlag GmbH & Co. KGaA

Silver is the most-often used metal material in superlens applications due to the fact that it exhibits the lowest on-resonance loss of any natural noble metal at optical frequencies [22, 23]. Pure-silver superlenses [11], however, have the drawback that they can satisfy the superlensing condition only at one wavelength, which is typically in the ultraviolet range. Other materials could be used in place of silver in order to shift the operational wavelength [16], but the choices are actually quite limited due to the finite number of elemental materials and the fact that dispersion in natural materials is not adjustable. Hence, it is often impossible to find a suitable natural material that shows a plasmonic resonance and hence superlensing behavior at a desired wavelength while simultaneously showing low loss.

One method of overcoming this issue was proposed recently by W.S. Cai et al. [17] and Z.T. Liu et al. [18], who showed that a metal-dielectric composite could be used to create a superlens at any desired wavelength within a broad range by adjusting the volume filling fraction of the constituent materials. Their work was based on an Bruggeman effective-medium model [17,24] of a silver-silica composite whose silver nanoparticle sizes were deeply subwavelength, allowing the creation of a dilute metal with an adjustable permittivity. By tailoring the silver filling fraction, the superlensing condition can be satisfied for any wavelength in the visible and near-IR range.

However, such nanocomposites often exhibit high surface roughness, which limits their overall imaging capabilities by decreasing the ultimate resolution achievable by the superlens. In fact, even with pure-metal superlenses this is a problem [11, 15]. Experimental results show that sub-diffraction resolution requires a smooth and thin metal film from the fabrication process [14, 15]. When the root-mean-squared (RMS) roughness of the silver film is higher than 1 nm, the superlens resolution suffers markedly [14, 15]. However, recent work has shown promise in using a germanium (Ge) wetting layer during the fabrication process to reduce the pure Ag film surface roughness [14, 25, 26]. In this work, we investigate the possibility of reducing the roughness of a silver-silica composite superlens through the addition of an ultrathin Ge layer. Specifically, we examine the effects of adding a Ge layer on the roughness and optical properties of silver-silica nanocomposite films.

2. Sample fabrication

To study the smoothing effects of a thin Ge layer, silver-silica random nanocomposite films have been fabricated by depositing multiple semicontinuous Ag and SiO_2 layers on glass and Si(100) substrates pre-coated with Ge/SiO_2 or SiO_2. All of the samples were fabricated using an electron-beam evaporation system (CHA Industries Model 600) with a base pressure in the chamber of about 1×10^{-6} Torr (1.33×10^{-4} Pa). Silver (99.9999%, Alfa Aesar), germanium (99.999%, Cerac), and SiO_2 (99.995%, Kurt J. Lesker Corp.) source materials were used to fabricate the samples. The evaporation rates were 0.05 nm/s for Ag and Ge and 0.1 nm/s for SiO_2. The deposition rates were monitored in real time with a quartz crystal oscillator, and hence all quoted layer thicknesses herein are actually mass average thicknesses. The initial glass and silicon substrates were cleaned using several steps, including multiple solvent rinses, a piranha (H_2O_2:$3H_2SO_4$) acid bath, several ultrapure water rinses and drying with pressurized gaseous nitrogen.

The samples fabricated on silicon wafers were used for high-resolution SEM and AFM imaging and spectroscopic ellipsometry measurements, while those fabricated on glass substrates were used for far-field spectral measurements. A 10-nm SiO_2 layer and a very thin Ge layer ($0.5-2.0$ nm) were deposited on the Si wafer and glass substrates to form Ge/SiO_2/Si and Ge/SiO_2/glass substrates. Then several paired SiO_2/Ag layers were deposited on the prepared substrates. We describe these layers as $(SiO_2/Ag)_n$, where n is the number of SiO_2/Ag pairs. The $(SiO_2/Ag)_n$ layers were deposited sequentially on the substrate without breaking the chamber vacuum. In these studies, we varied both the number of paired SiO_2/Ag layers and their thicknesses.

3. Single-paired SiO_2/Ag composite films

We first studied a group of single-paired SiO_2/Ag composite films with a Ge sub-layer, a simple case of $(SiO_2/Ag)_n$ nanocomposite films. In order to characterize the surface morphologies of our samples and determine the effect of the Ge sub-layer on the final film roughness, we performed extensive atomic force microscope (AFM) studies of the prepared samples. The surface morphologies were observed at room temperature using a Veeco Dimension 3100 AFM in a non-contact, tapping mode with a scan size of 1×1 μm^2, a scan rate of 1 Hz and standard pyramidal Si tapping-mode AFM tips. The collected AFM topographs were characterized by computing the RMS roughness values from each image.

Table 1 shows the Ge thicknesses and RMS roughness values of a group of single-paired, 5 nm SiO_2/5 nm Ag composite films on Ge/SiO_2/Si substrates. The thickness of the SiO_2 under the Ge layer was 10 nm, while the Ge thickness varies between 0 and 2 nm. Comparing the RMS roughness values of Samples #1 through #4 allows us to discern the effect of adding a thin Ge layer to a simplified composite structure. Samples #2, #3, and #4 (5 nm SiO_2/5 nm Ag on Ge/SiO_2/Si(100) substrates, where Ge thickness varies from 0.5 to 2 nm) exhibit much lower roughness than Sample #1 (5 nm SiO_2/5 nm Ag on a SiO_2/Si(100) substrate) due to the influence of the Ge layer. The measured RMS roughness values of Samples #2, #3, and #4 (with Ge) were only around $0.175-0.35$ nm, while that of Sample #1 (without Ge) was 1.04 nm.

© 2010 by Astro Ltd.
Published exclusively by WILEY-VCH Verlag GmbH & Co. KGaA

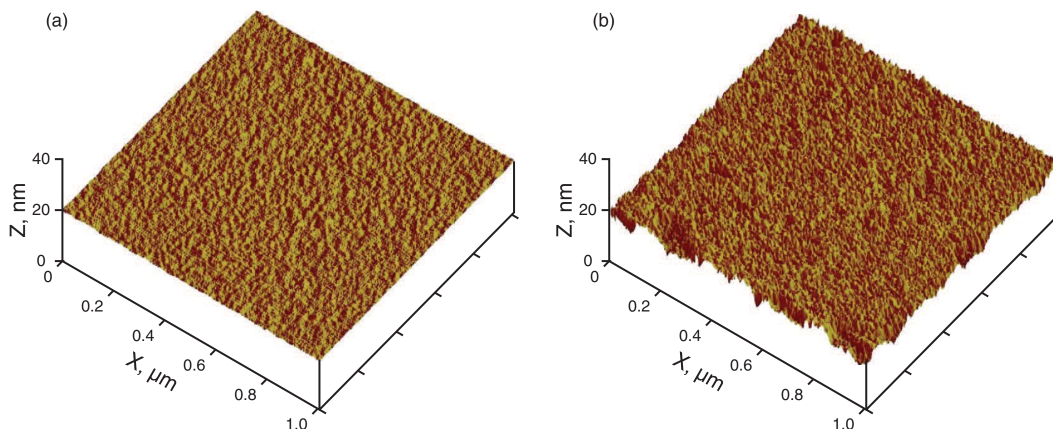

Figure 1 (online color at www.lphys.org) Representative surface morphologies from AFM topographs: (a) – 5 nm SiO_2/5 nm Ag composite film on a Ge/SiO_2/Si(100) substrate (Sample #4 of Table 1). (b) – the same composite layers on a SiO_2/Si(100) substrate (Sample #1 of Table 1)

Sample number	#1	#2	#3	#4
Ge thickness	0	0.5	1	2
RMS roughness	1.04	0.35	0.175	0.20

Table 1 Fabrication parameters and RMS roughness values of single-paired, 5 nm SiO_2/5 nm Ag composite films on Ge/SiO_2/Si substrates. The thickness of the SiO_2 under the Ge is 10 nm, while the Ge thickness varies between 0 and 2 nm (all values in nm)

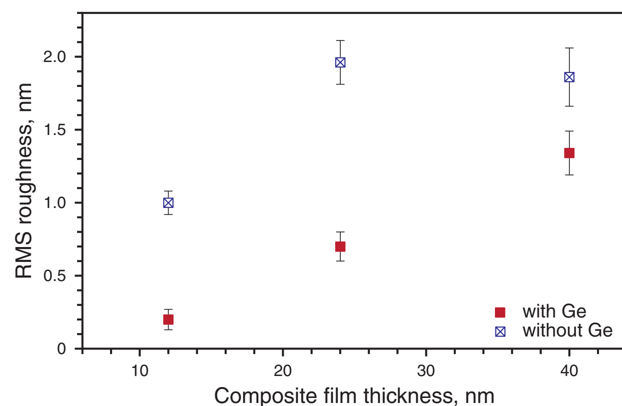

Figure 2 (online color at www.lphys.org) Comparison of measured surface roughness values for $(SiO_2/Ag)_n$ composite films with and without a Ge layer. The filling factor of Ag is 0.5 for all the samples

Typical surface morphologies of Samples #1 and #4 obtained from AFM topographs are shown in Fig. 1. The AFM images are shown at the same scan size and with the same height scale for ease of comparison. In this figure, we can see that the 5 nm SiO_2/5 nm Ag composite film on a Ge/SiO_2/Si(100) substrate (Sample #4, Fig. 1a) is visibly smoother than the same composite film without Ge (Sample #1, Fig. 1b). Combined with the roughness measurements, we therefore conclude from this data that the inclusion of an ultrathin Ge layer below the SiO_2/Ag composite layer greatly improves the surface roughness of the single-paired SiO_2/Ag composite film.

We can also compare the RMS roughness of Samples #2, #3, and #4 to determine the influence of the Ge layer thickness on the surface roughness of a simplified composite film structure. It is clear from Table 1 that, for single-paired composite films, the roughness of SiO_2/Ag composite films doesn't significantly change for Ge sub-layer thicknesses greater than 0.5 nm. In our studies, we actually found that the smoothing effect of the Ge layer saturates at a thickness of about 0.5 nm. We take this effect as a sign that the deposited Ge has formed a continuous layer at a mass average thickness of about 0.5 nm, and additional Ge therefore would not alter the overall roughness of the simple composite structure. This saturation effect has also been shown for Ge sub-layers below continuous, pure silver films [25] and is also presented for the multilayer $(SiO_2/Ag)_n$ nanocomposite films.

4. Multi-layer $(SiO_2/Ag)_n$ composite films

4.1. Surface roughness analysis

We next studied the effect of a 2-nm Ge sub-layer on the properties of multi-layer, $(SiO_2/Ag)_n$ composite films. We again used AFM analysis techniques to study the surface morphologies of a group of fabricated samples. Fig. 2 shows the surface roughness comparison for several

© 2010 by Astro Ltd.
Published exclusively by WILEY-VCH Verlag GmbH & Co. KGaA

Sample number	Ag filling fraction	Ag sub-layer thickness, nm	SiO_2 sub-layer thickness, nm	Paired Ag/SiO_2 layers	Total film thickness, nm	RMS roughness
#5	0.67	4	2	2	12	0.4
#6	0.67	4	2	4	24	1.2
#7	0.67	4	2	4	36	1.8

Table 2 Fabrication parameters and RMS roughness values of multi-layer, $(SiO_2/Ag)_n$ composite films on 2 nm Ge/10 nm SiO_2/Si substrates with varied total film thicknesses

Sample number	Ag filling fraction	Ag sub-layer thickness, nm	SiO_2 sub-layer thickness, nm	Paired Ag/SiO_2 layers	Total film thickness, nm	RMS roughness
#8	0.50	4	4	3	24	0.7
#6	0.67	4	2	4	24	1
#9	0.71	4	1.6	4	11.4	1.3
#10	0.80	4	1	4	20	1.4

Table 3 Fabrication parameters and RMS roughness values of multi-layer, $(SiO_2/Ag)_n$ composite films on 2 nm Ge/10 nm SiO_2/Si substrates with varied Ag filling fractions

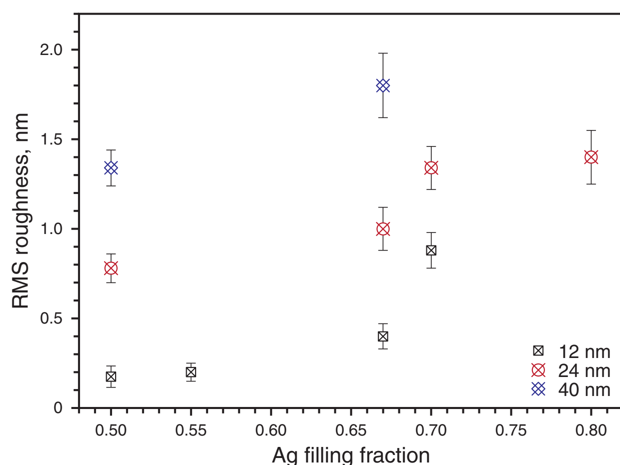

Figure 3 (online color at www.lphys.org) Measured RMS roughness values for multi-layer $(SiO_2/Ag)_n$ composite films for various Ag filling fractions and total film thicknesses

$(SiO_2/Ag)_n$ composite films (total thicknesses of 12 nm, 24 nm, and 40 nm) with and without a Ge layer. The Ag filling fraction is 0.5 for all the samples presented here. Fig. 2 clearly shows that the surface roughness of the multi-layer, $(SiO_2/Ag)_n$ composite films decreases when a 2-nm Ge sub-layer is included in the fabrication process.

We extended our analysis of composite $(SiO_2/Ag)_n$ films with Ge layers by varying the fabrication parameters of the composites. We studied the smoothing effect of a 2-nm Ge layer on composite films with different total composite film thicknesses and different Ag filling fractions. As before, we characterized these samples using AFM and obtained the RMS roughness results, which are shown in Table 2 and Table 3.

Table 2 shows the comparison of the surface roughness for a group of samples with different total composite film thicknesses. We see that at a constant Ag filling fraction, the RMS roughness increases with increasing total film thickness. Table 3 shows the comparison of the surface roughness of a group of samples with varying Ag filling fractions. To create samples with different filling fractions, we adjusted the thicknesses of the SiO_2 sub-layers from 1 nm to 4 nm while keeping the thicknesses of the Ag sub-layers fixed at 4 nm in each paired SiO_2/Ag layer. As shown in Table 3, the RMS surface roughness of the overall composite increases when the Ag filling fraction increases. For clarity, the measured RMS roughness values of composite samples with varied Ag filling fractions and total film thicknesses are shown in Fig. 3. The trends in our data suggest that lower total film thicknesses and lower metal filling fractions provide relatively better smoothing effects.

4.2. SEM analysis

We can also gain some insight into the structure of our samples by obtaining and studying scanning electron microscope (SEM) images of the multi-layer, $(SiO_2/Ag)_n$ composite films. The fabrication parameters and roughness values of these films are shown in Table 4.

Fig. 4a shows the SEM image of a (6 nm SiO_2/6 nm $Ag)_2$ film (Sample #11) on a Ge/SiO_2/Si(100) substrate, while Fig. 4b shows the SEM image of a (4 nm SiO_2/4 nm $Ag)_3$ film (Sample #8) on the same type of substrate. These two samples have the same Ag filling fraction (0.5) and

© 2010 by Astro Ltd.
Published exclusively by WILEY-VCH Verlag GmbH & Co. KGaA

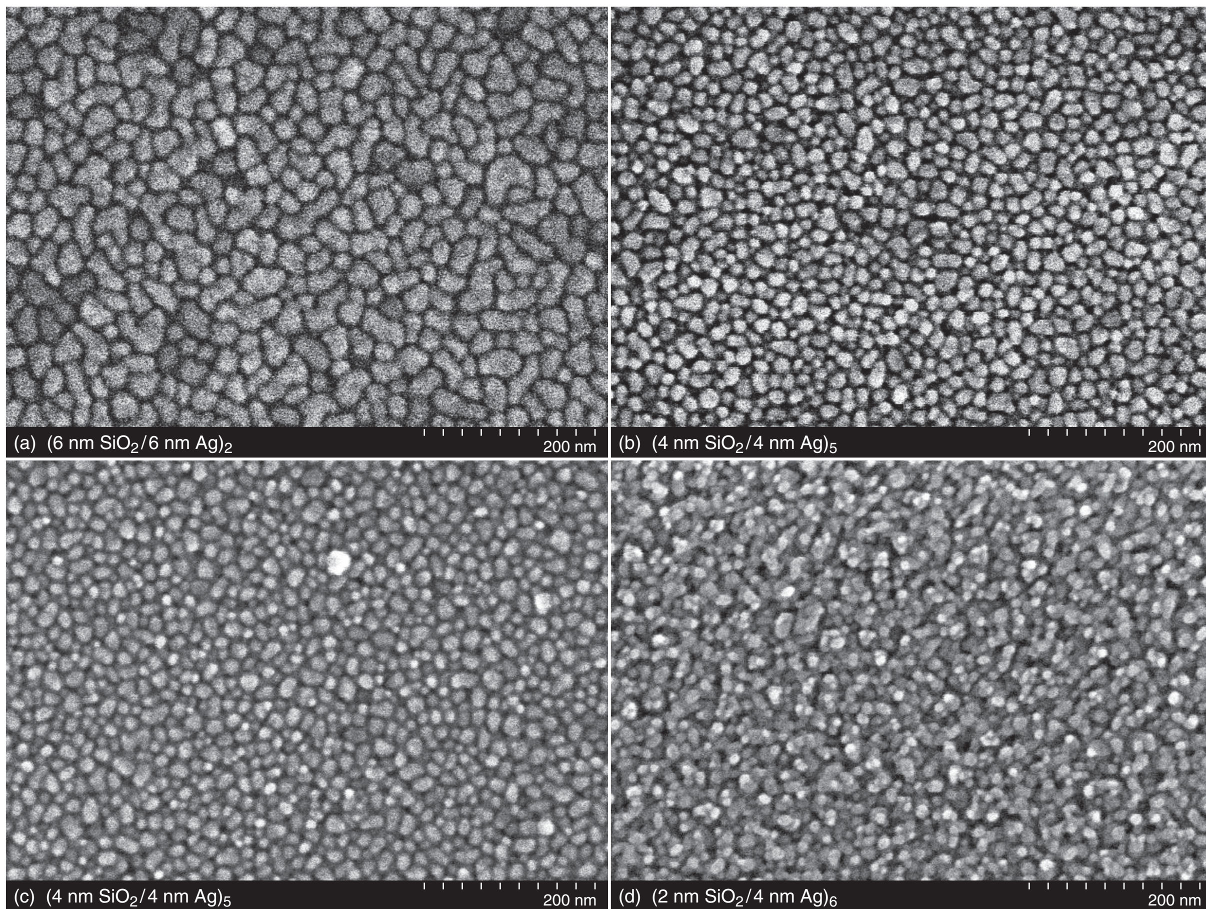

Figure 4 (online color at www.lphys.org) SEM images of multi-layer, (SiO2/Ag)n composite films on Ge/SiO2/silicon(100) substrates. (a) – sample #11 (6 nm SiO2/6 nm Ag)$_2$, RMS roughness is 0.85 nm ; (b) – sample #8 (4 nm SiO2/4 nm Ag)$_3$, RMS roughness is 0.7 nm; (c) – sample #12 (4 nm SiO2/4 nm Ag)$_5$, RMS roughness is 1.34 nm; (d) – sample #7 (2 nm SiO2/4 nm Ag)$_6$, RMS roughness is 1.85 nm

Sample number	Ag filling fraction	Ag sub-layer thickness, nm	SiO_2 sub-layer thickness, nm	Paired Ag/SiO_2 layers	Total film thickness, nm	RMS roughness
#11	0.50	6	6	2	24	0.85
#8	0.50	4	4	3	24	0.70
#12	0.50	4	4	5	40	1.34
#7	0.67	4	2	6	36	1.85

Table 4 Fabrication parameters and RMS roughness values of multi-layer, $(SiO_2/Ag)_n$ composite films on 2 nm Ge/10 nm SiO_2/Si substrates with varied Ag filling fractions

total film thickness (24 nm) but different sub-layer thicknesses. These SEM images show that, on average, smaller silver cluster sizes are created when the Ag and SiO_2 sub-layer thicknesses are thinner. Looking at the roughness values for each film in Table 4 then leads us to the conclusion that the overall composite film is smoother for smaller silver cluster sizes.

Fig. 4c shows the SEM image of a (4 nm SiO_2/4 nm Ag)$_5$ film (Sample #12) on a Ge/SiO_2/Si(100) substrate. The samples imaged in Fig. 4c and Fig. 4b have the same Ag filling fraction (0.5) and sub-layer thicknesses (4 nm SiO_2/4 nm Ag) but different total film thicknesses. Comparing Fig. 4c with Fig. 4b, we see that the silver cluster sizes are quite similar when the sub-layer thicknesses are

© 2010 by Astro Ltd.
Published exclusively by WILEY-VCH Verlag GmbH & Co. KGaA

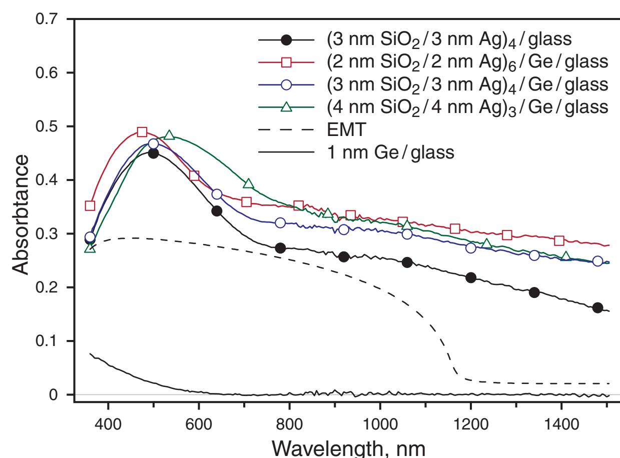

Figure 5 (online color at www.lphys.org) Absorptance comparison of samples with different sub-layer thicknesses. All the composite films have a total film thickness of 24 nm and a silver filling fraction of 0.5

the same even though the total thicknesses of the samples may be different.

The films shown in panels (c) and (d) of Fig. 4 differ primarily in their Ag filling fractions. The two films were deposited with the same Ag sub-layer thickness but different SiO_2 sub-layer thicknesses. The SiO_2 sub-layer thickness is thinner for Sample #7 (Fig. 4d) than for Sample #12 (Fig. 4c). Comparing the images of these two films, we see that the film in Fig. 4d with a higher Ag filling fraction has less uniformity in its silver cluster morphology. The silver clusters show a variety of sizes in Fig. 4d, while they are more uniform in size in Fig. 4c.

4.3. Analysis of optical properties

To better understand the optical properties of the composite films, we measured the far-field spectral responses of a group of samples deposited on Ge/SiO_2/glass substrates. The spectral responses (transmittance and reflectance) of the films were measured using a PerkinElmer Lambda 950 UV-Vis-NIR spectrophotometer with an integrating sphere accessory. The absorptance values were obtained through the calculation: absorptance (A) = 1 – transmittance (T) – reflectance (R).

Fig. 5 shows the absorptance of samples that have the same filling fraction (0.5) and total film thickness (24 nm) but different sublayer thicknesses. The dashed line in Fig. 5 shows the calculated absorptance of a silver-silica composite film whose filling fraction is 0.5 and total film thickness is 24 nm, based on the Bruggeman effective-medium theory (EMT) [24]. The EMT result shows a broad absorption band while the measured spectra of composite films with sublayer thicknesses of 2 nm, 3 nm, and 4 nm show much narrower absorption bands. The measured absorptance peaks are determined by the localized surface plasmon resonance of the Ag particles when the condition $\varepsilon'_M(\omega) = -2\varepsilon'_H(\omega)$ is satisfied. $\varepsilon'_M(\omega)$ and $\varepsilon'_H(\omega)$ are the real parts of the metal (Ag) permittivity and host material (SiO_2) permittivity in composites [24, 27–29]. The localized surface plasmon resonance shifts toward longer wavelengths with increasing sub-layer thicknesses.

Fig. 5 also shows that a (3 nm SiO_2/3 nm Ag)$_4$ composite film with a 1-nm Ge sub-layer layer tends to exhibit stronger absorptance than that of the same composite film directly deposited on a glass substrate. Due to the extremely small thickness of the sub-layer, the contribution from the Ge layer to the total absorption is not significant. The solid line in Fig. 5 shows the measured absorptance from a 1-nm Ge/glass sample. The absorptance from the 1-nm Ge layer is very small, particularly when the operation wavelength is beyond 600 nm. Hence, it can be concluded that the additional absorption of samples with a Ge layer is mainly from the composite itself. This may be indicative of structural changes in the film – more fractal-like structures would produce broader absorptance bands in a metal-dielectric composite film [24].

We also obtained spectroscopic ellipsometry (SE) measurements for our samples via a variable-angle spectroscopic ellipsometer (J.A. Woollam Vertical VASE) over the spectral range of 360 – 1500 nm. The measurements were performed in steps of 10 nm at three different incidence angles of 50°, 60°, and 70°. The measured ellipsometric angle data (Ψ, Δ) were analyzed and fitted to a generic oscillator model that included a Drude function, a Gaussion function, and a Tauc-Lorentz function. Based on the fitting, the effective electric permittivities of the composites were retrieved and are shown in Fig. 6. For SE measurements, all data was collected using the films that were deposited on Ge/SiO_2/Si(100) substrates. The total thicknesses are all 24 nm, the filling fractions are all 0.5, and the sub-layer thicknesses are 2 nm, 3 nm, and 4 nm.

Fig. 6 shows that the retrieved real parts (ε') and imaginary parts (ε'') of the effective electric permittivities do not match the calculated EMT results using the permittivity values of bulk Ag (Johnson & Christy data [22]) and silica. According to the EMT, the effective permittivity of the composites should be unique if the constituent materials and their filling fraction within the composites fraction are fixed. However, our measured results show that composites with different sublayer thicknesses (different cluster sizes) may have different effective permittivity, even though the constituent materials and their filling fraction within the composites fraction are fixed.

Our retrieved ε' values, though qualitatively similar to the EMT values, show smaller magnitudes than the bulk-silver EMT result (black, dashed line). In addition, the retrieved ε'' values have much narrower absorption bands and generally far higher magnitudes than the theoretical result. We conclude, therefore, that the unmodified

© 2010 by Astro Ltd.
Published exclusively by WILEY-VCH Verlag GmbH & Co. KGaA

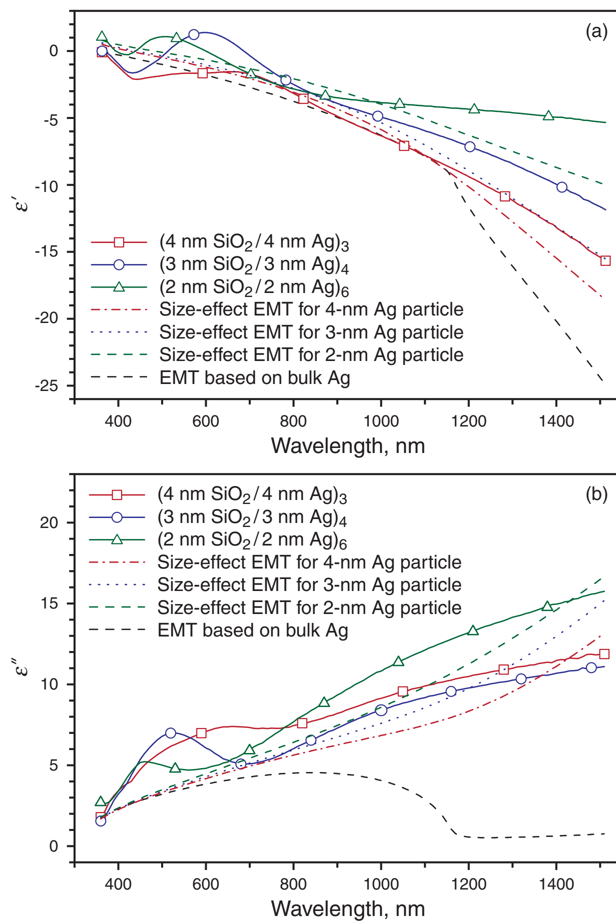

Figure 6 (online color at www.lphys.org) Retrieved effective electric permittivities of composites with different sub-layer thicknesses. All the composite films have a total film thickness of 24 nm and filling fraction of 0.5. EMT and modified size-effect EMT predictions are shown for comparison

Bruggeman EMT formulation is not suitable for predicting accurate responses for our nanocomposite films. The EMT does not include the influence of the nanostructures of the composites, such as the particle sizes and shapes, in the calculation of the effective permittivity. In addition, the EMT formulation provides a unique effective electric permittivity for all metal-dielectric composites that have the same constituents and metal filling fractions, even though they may have different nanostructures inside the composites. However, this simple assumption turns to be incorrect for real metal-dielectric nanocomposites. In our compsites, small Ag particles embedded in the dielectric material lead to localized surface plasmon resonances. The narrow absorption bands (around 400 — 600 nm) of our measured results shown in Fig. 6 are a consequence of the localized surface plasmon resonance of the small Ag particles within the nanocomposite (also see the SEM images of Fig. 4). Note that the data in Fig. 6 also indicate that the resonance position shifts toward longer wavelengths when the silver sub-layer thickness is increased; this is a sign that the silver has formed larger clusters on average. On the contrary, the localized surface plasmon resonance absorption is not clearly shown in the EMT predictions.

Moreover, the measured and calculated results beyond the absorption band do not match each other either. The black, dashed line in Fig. 6b shows the calculated effective permittivity of a composite film based on EMT using the Johnson & Christy values [22] of bulk silver. The curve indicates that the imaginary part of the effective electric permittivity should drop substantially and remain close the bulk-silver values for wavelengths beyond the surface plasmon absorption band. However, the retrieved ε'' of our composites do not decrease as drastically as the EMT predicts; rather, they continuously increase for increasing wavelengths, reaching values for ε'' as high as 10 – 15. Hence, we conclude that the Ag nanoparticles within the composite actually exhibit a much larger loss than the bulk material due to the quantum size effect.

The Ag dielectric function can be described using the Drude model, as shown in Eq. (1).

$$\varepsilon = \varepsilon_1 - \frac{\omega_p^2}{\omega^2 + i\gamma_p\omega} \,. \tag{1}$$

Here $\varepsilon_1 = 2.1485$ is a dielectric constant, $\omega_p = 9.1821$ eV is the plasma frequency, and γ_p is the damping constant, which is a determine factor for the Ag loss. When the Ag particles become extreme small, the damping constant (γ_p) is no longer a constant but a size-dependent parameter due to the quantum size effect. Hence, an additional size-dependent term should be included in the damping constant [23, 26, 30, 31]:

$$\gamma_p = \gamma_\infty + A\frac{\upsilon_F}{R} \,, \tag{2}$$

where $\gamma_\infty = 0.021$ eV is assumed a constant for bulk Ag, $\upsilon_F = 1.39 \times 10^6$ m/s is the Fermi velocity, *R* is the metal particle radius or grain size, and the *A*-parameter is a constant around one that depends on the details of the scattering processes and the kind of medium surrounding the particle. We use $A = 1.3$ here for Ag particles fully embedded in silica [31]. We thereby found the damping constants γ_p for 2-nm, 3-nm, and 4-nm Ag particles embedded in silica to be 0.41 eV, 0.54 eV, and 0.8 eV, respectively. These values are much larger than the 0.021 eV value for bulk Ag. Using the modified permittivity of the Ag particles, we recalculated the effective permittivity of our silver-silica composite films through EMT. For the imaginary parts of the revised permittivities, the modified results are much higher than those predicted via bulk Ag values. The size-effect EMT results have been included in Fig. 6, which are closer to the measured values of our real samples for wavelengths beyond the absorption band, even though the localized surface plasmon resonances of the Ag particles are still not predicted in the EMT results.

© 2010 by Astro Ltd.
Published exclusively by WILEY-VCH Verlag GmbH & Co. KGaA

5. Summary

In summary, we have performed a number of experiments related to the fabrication and characterization of near-field superlens composite prototypes. We have primarily focused on minimizing the top surface roughness of the composite by including a very thin germanium layer in the deposition procedure. Using the ultrathin Ge layer below our multi-layer $(SiO_2/Ag)_n$ composite films significantly reduced the final surface roughness. However, we have also found that this smoothing effect can be weakened when either the total film thickness or the Ag filling fraction is increased. Our experimental results show that the RMS roughness of a composite film can be reduced to less than 1 nm when the total thickness of the composite film is below 24 nm and the Ag filling fraction is under 0.7. Additionally we have observed that silver-silica nanocomposite films fabricated on a Ge sub-layer show quite different spectra from those predicted by EMT in the visible and near-IR wavelength ranges. The effective permittivities of the composites are no longer unique if only the constituent materials and their filling fraction within the composites fraction are fixed. The nanostructures inside the composite also have a significant influence on the optical response of the composites.

Overall, our results indicate that, compared to multilayer, $(SiO_2/Ag)_n$ composite films deposited without a Ge layer, it is possible to produce smoother silver-silica nanocomposite films when including an ultrathin germanium layer in the fabrication process. The discrepancy between the experimental results and EMT predictions of metal-dielectric nanocomposites should lead to further studies on the effect of the nanostructure of the composites of the optical properties of such composites. We anticipate these results to be of particular interest to researchers studying metamaterials such as advanced superlenses.

Acknowledgements This work was partially supported by the Army Research Office under Multidisciplinary University Research Initiative (ARO-MURI) contract 50342-PH-MUR and W911NF-09-1-0539, and by the National Science Foundation Partnership for Research and Education in Materials (PREM) grant DMR 0611430.

References

[1] D.R. Smith, J.B. Pendry, and M.C.K. Wiltshire, Science **305**, 788 (2004).
[2] V.M. Shalaev, Nat. Photonics **1**, 41 (2007).
[3] W. Cai and V. Shalaev, Optical Metamaterials: Fundamentals and Applications (Springer, New York, 2009).
[4] A. Boltasseva and V.M. Shalaev, Metamaterials **2**, 1 (2008).
[5] N.M. Litchinitser and V.M. Shalaev, Laser Phys. Lett. **5**, 411 (2008).
[6] I.I. Smolyaninov, Laser Phys. Lett. **7**, 259 (2010).
[7] A.K. Popov, V.V. Slabko, and V.M. Shalaev, Laser Phys. Lett. **3**, 293 (2006).
[8] K. Nouneh, I.V. Kityk, K. Michalska-Małecka, K. Ozga, V.T. Adamiv, Ya.V. Burak, and I.M. Teslyuk, Laser Phys. **18**, 965 (2008).
[9] D.O. Saparina and A.P. Sukhorukov, Laser Phys. **19**, 1125 (2009).
[10] J.B. Pendry, Phys. Rev. Lett. **85**, 3966 (2000).
[11] N. Fang, H. Lee, C. Sun, and X. Zhang, Science **308**, 534 (2005).
[12] D.O.S. Melville, R.J. Blaikie, and C.R. Wolf, Appl. Phys. Lett. **84**, 4403 (2004).
[13] D. Melville and R. Blaikie, Opt. Express **13**, 2127 (2005).
[14] P. Chaturvedi, W. Wu, V.J. Logeeswaran, Z.N. Yu, M.S. Islam, S.Y. Wang, R.S. Williams, and N.X. Fang, Appl. Phys. Lett. **96**, 043102 (2010).
[15] H. Lee, Y. Xiong, N. Fang, W. Srituravanich, S. Durant, M. Ambati, C. Sun, and X. Zhang, New J. Phys. **7**, 255 (2005).
[16] T. Taubner, D. Korobkin, Y. Urzhumov, G. Shvets, and R. Hillenbrand, Science **313**, 1595 (2006).
[17] W.S. Cai, D.A. Genov, and V.M. Shalaev, Phys. Rev. B **72**, 193101 (2005).
[18] Z.T. Liu, M.D. Thoreson, A.V. Kildishev, and V.M. Shalaev, Appl. Phys. Lett. **95**, 033114 (2009).
[19] H.-K. Yuan, U.K. Chettiar, W.S. Cai, A.V. Kildishev, A. Boltasseva, V.P. Drachev, and V.M. Shalaev, Opt. Express **15**, 1076 (2007).
[20] A.V. Kildishev and V.M. Shalaev, Opt. Lett. **33**, 43 (2008).
[21] V.M. Shalaev, Science **322**, 384 (2008).
[22] P.B. Johnson and R.W. Christy, Phys. Rev. B **6**, 4370 (1972).
[23] V.P. Drachev, U.K. Chettiar, A.V. Kildishev, H.-K. Yuan, W.S. Cai, and V.M. Shalaev, Opt. Express **16**, 1186 (2008).
[24] V.M. Shalaev (ed.), Optical Properties of Nanostructured Random Media (Springer, Berlin – Heidelberg, 2002).
[25] V.J. Logeeswaran, N.P. Kobayashi, M.S. Islam, W. Wu, P. Chaturvedi, N.X. Fang, S.Y. Wang and R.S. Williams, Nano Lett. **9**, 178 (2009).
[26] W.Q. Chen, M.D. Thoreson, S. Ishii, A.V. Kildishev, and V.M. Shalaev, Opt. Express **18**, 5124 (2010).
[27] V.A. Podolskiy, A.K. Sarychev, E.E. Narimanov, and V.M Shalaev, J. Opt. A **7**, S32 (2005).
[28] U.K. Chettiar, A.V. Kildishev, T.A. Klar, and V.M. Shalaev, Opt. Express **14**, 7872 (2006).
[29] S. Yoshida, T. Yamaguchi, and A. Kinbara, J. Opt. Soc. Am. **61**, 62 (1971).
[30] A. Pinchuk, U. Kreibig, and A. Hilger, Surf. Sci. **557**, 269 (2004).
[31] A. Hilger, M. Tenfelde, and U. Kreibig, Appl. Phys. B **73**, 361 (2001).

© 2010 by Astro Ltd.
Published exclusively by WILEY-VCH Verlag GmbH & Co. KGaA